PAPER

Mitigating waveguide loss in Ge–Sb–Se chalcogenide glass photonics

IOP Publishing Journal of Physics D: Applied Physics
J. Phys. D: Appl. Phys. **57** (2024) 305107 (6pp) https://doi.org/10.1088/1361-6463/ad43f5

Mitigating waveguide loss in Ge–Sb–Se chalcogenide glass photonics

Fengbo Han[1,2,3], Yunfei Niu[1,3], Yan Zhang[1], Jue Gong[1], Shaoliang Yu[1] and Qingyang Du[1,*]

[1] Zhejiang Lab, Hangzhou, Zhejiang 311121, People's Republic of China
[2] Fujian Key Laboratory of Ultrafast Laser Technology and Applications, School of Electronic Science and Engineering, Xiamen University, Xiamen, Fujian 361005, People's Republic of China

E-mail: qydu@zhejianglab.edu.cn

Received 6 February 2024, revised 21 March 2024
Accepted for publication 26 April 2024
Published 8 May 2024

Abstract

Minimizing propagation loss within waveguides remains a central objective across diverse photonic platforms, impacting both linear lightwave transmission and nonlinear wavelength conversion efficiencies. Here, we present a method to mitigate waveguide loss in $Ge_{28}Sb_{12}Se_{60}$ chalcogenide glass, a material known for its high nonlinearity, broad mid-infrared transparency, and significant potential for mid-IR photonics applications. By applying a sacrifical oxide layer to eliminate etching residues and a subsequent waveguide thermal reflow to smooth lithography-induced line edge roughness, we successfully reduced the waveguide loss down to 0.8 dB cm^{-1} at 1550 nm wavelength. This represents the best result in small-core and high-index-contrast $Ge_{28}Sb_{12}Se_{60}$ channel waveguides. Our approach paves the way for low-loss, on-chip chalcogenide photonic devices.

Keywords: waveguide loss, chalcogenide glass, CMOS compatible process, thermal reflow

1. Introduction

Reducing propagation loss within planar waveguides has emerged as a persistent and critical focus. Low-loss waveguides contribute significantly to improved signal-to-noise ratios, higher detection sensitivities, and enhanced efficiency in light-matter interactions, which serves as the cornerstone for achieving optimal performance in diverse on-chip active and passive devices. To date, extensive research has explored technologies to mitigate the waveguide loss in various photonic flatforms, including silicon [1], silicon nitride [2], silicon carbide [3], germanium [4], and III–Vs [5]. Specifically, low-loss silicon nitride waveguides have reached a remarkably low 0.014 dB cm^{-1} value, which represents the lowest record among all planar waveguide platforms [6]. The successful demonstration of ultra-low loss in silicon nitride waveguides soon promotes several striking technologies, such as self-injection-locked turnkey soliton combs [7], highly coherent supercontinuums for tomography [8], and monolithic on-chip amplifiers [9].

While these material platforms have exhibited successful demonstrations in the near-IR, they become inevitably lossy when entering the mid-infrared (mid-IR) spectral regime due to phonon absorptions. The mid-IR regime holds immense potential for applications in chemical sensing, health monitoring, and spectroscopy due to the presence of numerous 'fingerprint' vibrational bands of molecules in this range [10]. On-chip solutions, facilitated by the emergence of CMOS-compatible technologies, address the growing demand for miniaturization and adherence to SWaP-C (size, weight, power, and cost) criteria for successful commercialization. However, in these devices, waveguide losses exert an inversely proportional impact on key performance metrics. Lower losses directly translate to enhanced sensitivity, reduced noise levels [11], lower thresholds for nonlinearities [12] and signal gain generation [13]. The huge impact of waveguide losses on such

[3] These authors contributed equally to this work.
[*] Author to whom any correspondence should be addressed.

devices drives the efforts for a low-loss photonic waveguide systems.

In this work, we demonstrate a systematic waveguide loss reduction study on $Ge_{28}Sb_{12}Se_{60}$ (GeSbSe) chalcogenide glass. Chalcogenide glass exhibits an extremely wide transparency window through the near-IR all the way to the long-wave IR [14–18] and is considered a practical waveguide material for mid-IR photonics. To date, there are several reports on low-loss chalcogenide glass waveguides with various compositions [19–23]. Compared with them, GeSbSe is highly nonlinear (vs. sulfide), less toxic, and immune to oxidation under ambient environment (vs. Arsenic-containing ones). To achieve low propagation loss, a clean and smooth waveguide must be garanteed. Here, we propose to adopt an oxide sacrificial layer for etch resist lift-off and a waveguide thermal reflow process in our waveguide fabrication. These processes involve introducing a thin oxide layer above the chalcogenide film which is subsequently removed after the etching process, and annealing the as-fabricated waveguide at elevated temperature to allow it to reflow. While the oxide sacrificial layer has been widely deployed as a hard etching mask or for forming special structures [24, 25], its application as an etch resist lift-off layer remains rare. Similarly, the use of thermal reflow to reduce surface roughness has mainly been observed in organic materials, such as polymer waveguides and photoresists [26, 27]. Although there have been a few reports to reflow chalcogenide glass waveguides, their losses are still much higher than 1 dB cm^{-1} [23, 28, 29]. In our work, we have successfully reduced the GeSbSe waveguide loss down to 0.8 dB cm^{-1} at 1550 nm wavelength by incorporating both steps into our fabrication flow. The result represents the lowest reported value in GeSbSe small-core and high-index-contrast ($\Delta n > 1$) nonlinear waveguides. It is worth noting that these two extra steps do not depend on specific waveguide geometry, and thus the process is equally applicable in making low-loss mid-IR photonic waveguides.

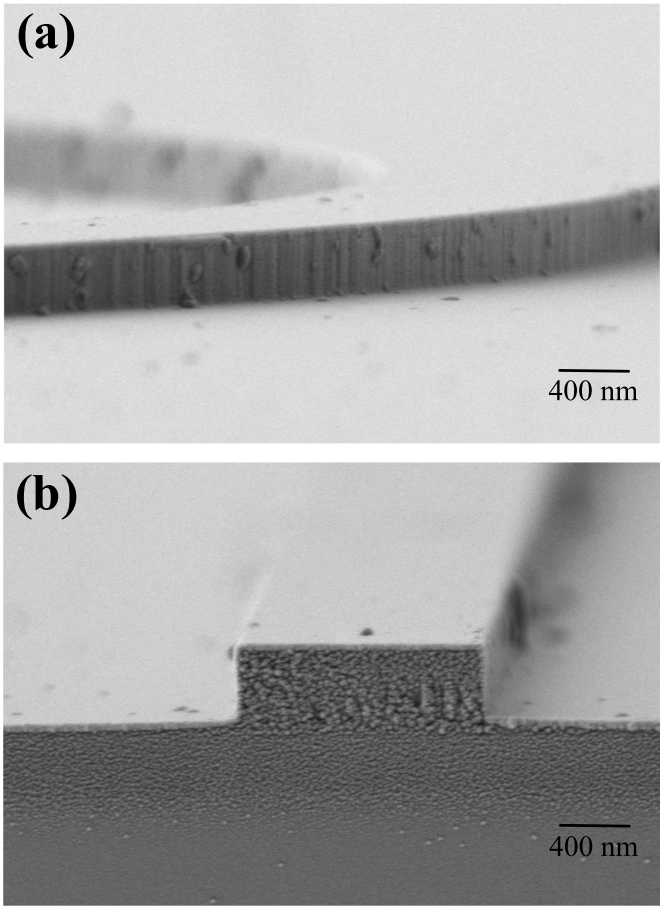

Figure 1. A representative SEM image of the as-fabricated waveguide (a) sidewall view; and (b) cross sectional view.

2. Waveguide fabrication and loss analysis

We fabricated the waveguide leveraging a foundry-compatible process. A 400 nm GeSbSe film was first thermally evaporated onto a 6″ silicon wafer with 3 μm oxide isolation cladding. The patterns were exposed by a Canon 3030EX6 KrF DUV stepper and etched with a Leuven ICP etcher. The etching chemistry was flourine-based, same as the previous established protocol [30]. The resist mask was removed by soaking the chip in an N-Methyl-2-pyrrolidone solution overnight. Figures 1(a) and (b) shows the SEM image of the as-fabricated waveguide. It is obvious that lithography-induced line edge roughness is clearly visible. Moreover, The resist residues are also scattered across the waveguide due to etch-induced degradation that makes the resist insoluble in the remover solution. Residues remaining after the etching process not only introduces scattering centers, leading to significant radiative losses, but also exhibits inherent absorptions due to the presence of hydrocarbonate bonds. We subsequently measured its waveguide loss through cut-back method and the result indicates an alarmly high loss of $\sim$10 dB cm^{-1} at 1550 nm wavelength.

Waveguide losses can be divided into several groups. First, material intrinsic absorption that arises from the Urbach tail near the band gap as well as mid-gap defects in amorphous solids are considered. A previous study with a chalcogenide glass microsphere resonator indicated a 0.002 dB cm^{-1} intrinsic loss was present [31]. Additionally, passivation flourocarbon coating at the waveguide sidewall also contributes to an overtone absorption of 0.1–1 dB cm^{-1} [32]. Radiative loss, arising from mode tunneling and waveguide bending, was next investigated. Based on our waveguide parameters: a 3 μm oxide spacer and bending radii exceeding 100 μm, modal analysis suggests negligible radiative loss due to sufficiently large confinement and curvature. The remaining loss is attributed to surface roughness-induced scattering, in which the smooth propagation of light is disrupted by uneven edges acting as scattering centers. These scattering losses become more pronounced in small-core waveguides where significant overlap exists between the light field and waveguide surfaces. It is worth emphasizing that the scattering loss takes up more than 90% of the total waveguide loss in our

waveguide, and therefore, in the next section, we focused on strategies for reducing waveguide surface roughness.

3. Towards a residue-free and smooth waveguide surface

3.1. Oxide sacrificial layer

It has been widely recognized that the etching residues are notoriously difficult to remove [33]. Our previous study with XPS revealed those residues to be flouro–carbonate-coated resists [19]. These coatings prevent further reaction of the resist to its remover solution and, furthermore, create an adhesion layer to the substrate, making those residues inert against chemical and even mechanical ultrasound sonication removing efforts. Some work has demonstrated successful elimination of residues with an extra round of oxygen plasma cleaning [34]. However, it is worth highlighting that chalcogenides, especially arsenic-containing ones, are susceptible to oxidation; adopting oxygen plasma may risk oxide formation and thus, leveraging this approach should be meticulously considered in the glass compositions. Thus, we propose to adopt an oxide sacrificial layer instead. A 50 nm-thick silicon dioxide was deposited prior to lithography via ICP-CVD at room temperature. In addition to isolating direct contact between the resist and the waveguide, this silicon dioxide layer also forms a hard etching mask, allowing high etching selectivity. After the ICP etch is completed, the chip is soaked in a diluted HF solution (5% concentration) to lift off the resist. We want to remark that for a fully etched waveguide, the HF solution also dissolves the buttom thermal oxide undercladding. Considering the ICP-CVD oxide is much less dense than the thermal oxide, the etch rate differs more than 10 times for these two layers, and consequently, merely small undercut was formed underneath the waveguide, which does not impact our waveguide structure. Figures 2(a) and (b) display SEM images of the waveguide top and sidewall, respectively. It clearly indicated that by adopting the oxide sacrificial layer, we were able to achieve a residue-free waveguide.

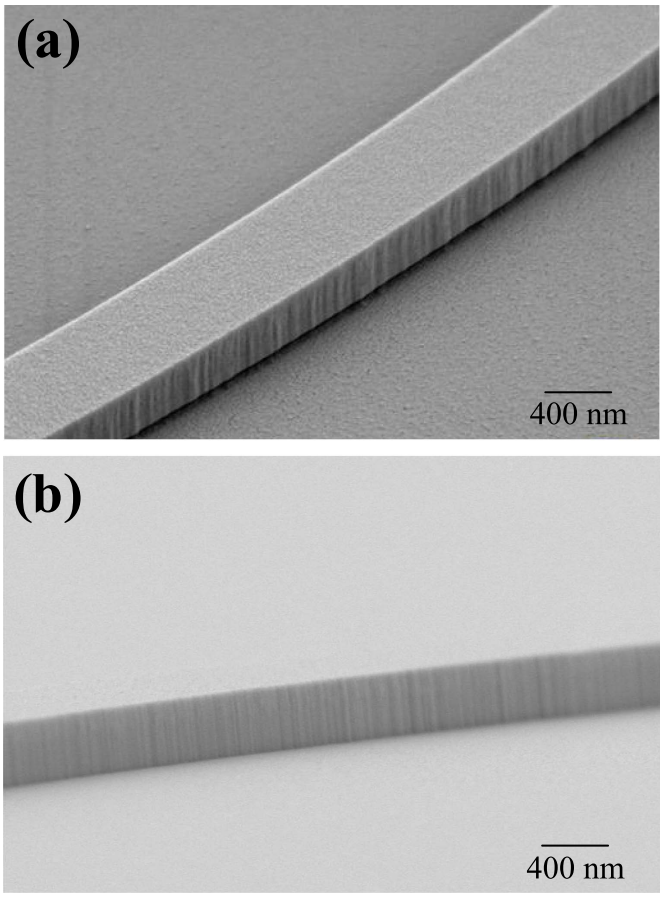

Figure 2. SEM images of (a) top surface and (b) sidewall of the waveguide fabricated with oxide sacrificial layer.

3.2. Waveguide thermal reflow

Although etching residues have been successfully eliminated thus far, there is still some line edge roughness caused by lithography, as shown in figure 2(b), which is another significant cause of scattering losses. It has been well established that thermal reflow is an effective approach to addressing surface roughness. When elevated to a temperature above its glass transition temperature T_g, the material enters the viscous flow regime, where it undergoes mass flow on a small scale. At abrupt corners, the local Gibbs energy is much higher compared to other flat places, contributing to a large surface tension. Consequently, this surface tension tends to round any uneven surfaces and create a smooth sidewall. The detailed kenetic theory of thermal reflow can be found in [23]. While many other works performed reflow mostly on resist, owing to the amorphous nature and the low T_g of chalcogenide glass, we were able to reflow directly on the glass waveguide. Reflowing the waveguide further flattens any etch-induced defect that guarantees enhanced smoothness of the sidewall. We wish to point out that there is indeed a previous report on the successful reflow of GeSbSe waveguide for loss reduction [29]. However, in this works, the reflow is so severe that the waveguide geometry changed from rectangular to cone-like. While this change is not harmful for light propagation, the geometry modification severely impacts the waveguide's dispersion as well as coupling characteristics, giving rise to disagreements over the corresponding behaviors to the designs. More importantly, this geometric change is difficult to predict, making it even harder for design compensation. Therefore, it is critical to preserve the waveguide geometry during the reflow. The thermal reflow process follows Arrhenius behavior. A reflow temperature that is too high can cause shape distortion or even dewetting, while a temperature that is too low may not be sufficiently thermally active to induce mass flow. Thus, we experimented with a reflow temperature of 260 °C and 300 °C for 3 min and characterized the waveguide roughness using a combination of SEM and AFM. Figures 3(a) through (f) shows the SEM images and AFM scans of the waveguide sidewall with no reflow, reflowed at 260 °C and at 300 °C, respectively. Since our waveguide sidewall is highly vertical, it is not possible for the AFM tip to acquire the sidewall roughness from scanning the top surface. The step at the waveguide edges

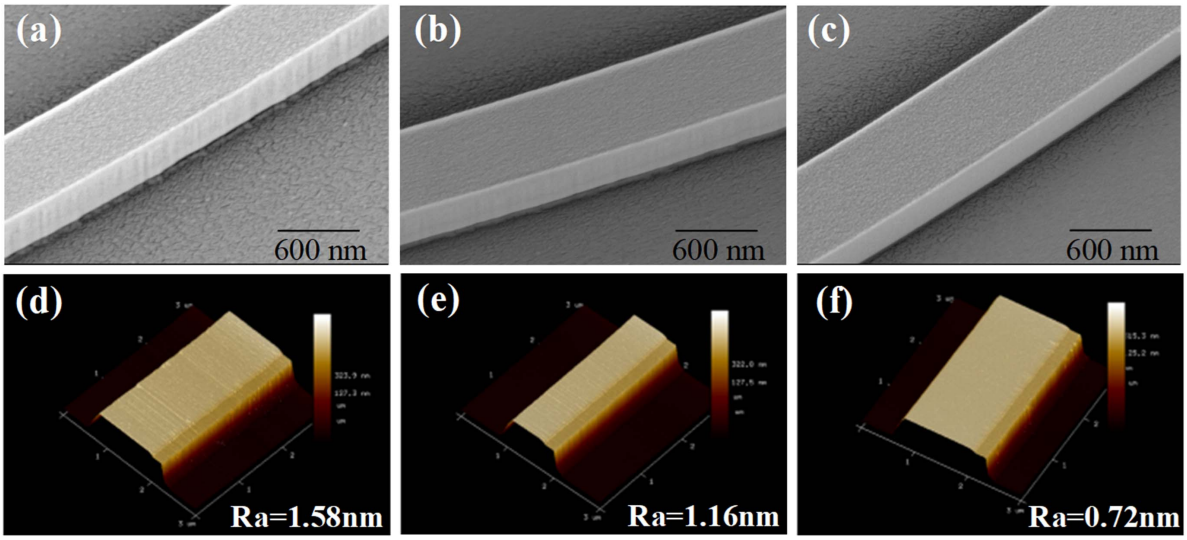

Figure 3. SEM of the waveguide under different reflow conditions. (a) Waveguide without reflow; (b) waveguide reflowed at 260 °C; and (c) waveguide reflowed at 300 °C. (d)–(f) Are corresponding AFM scan images.

displayed in the AFM plot are merely artifacts that should not be considered. Hence, we take only the surface roughness value as a reference. Our result has revealed a clearly discernible trend in sidewall roughness reduction with increased reflow temperature from the SEM images. AFM data also suggested an improvement in waveguide surface roughness from 1.58 nm to 0.72 nm. It is also worth highlighting that our waveguide geometry is well preserved after the reflow. The qualitative and quantitative results both strongly evidenced that waveguide thermal reflow is a viable route for producing a smooth waveguide.

4. Discussion

With the addition of an oxide sacrifical layer and waveguide thermal reflow, we were finally able to produce a residue-free and smooth sidewall waveguide. Its fabrication flow was summarized in figure 4. To examine possible material composition modifications during thermal reflow, EDS elemental analysis was performed and plotted in figure 5(a). Its material composition exhibits negligible change, demonstrating GeSbSe has high chemical stability under thermal reflow temperature. We subsequently tested the waveguide loss at 1550 nm wavelength leveraging the cut-back method. The fitted result, plotted in figure 5(b), suggested an attractively low loss of 0.8 dB cm^{-1}. To the best of our knowledge, it is the lowest ever reported in high index contrast and small core and high index contrast Ge–Sb–Se waveguide. To numerically simulate the sidewall roughness-induced scattering loss, we follow a simplified volume current method proposed by Payne and Lacey [35]. The model considers a planar waveguide with a sidewall roughness of σ and a corresponding correlation length of L_c. By calculating and collecting the radiative loss caused by sidewall roughness, the total scattering loss is obtained. According to our previous study, the waveguide sidewall roughness autocorrelation function follows an

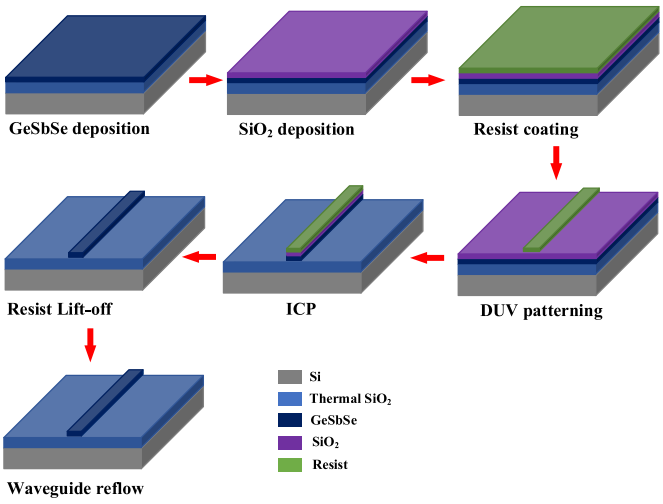

Figure 4. Schematic drawing of complete waveguide fabrication process flow incorporating oxide sacrificial layer and waveguide reflow.

exponential relation [19]. Thus, the loss term can be expressed by equation (1):

$$\alpha = \frac{\sigma^2}{\sqrt{2}k_0 d^4 n_1} g\left(n_1, n_2\right) f_e\left(n_1, n_2, L_c\right) \tag{1}$$

where α is waveguide loss, σ is the roughness mean square deviation value, k_0 denotes the propagation constant under vacuum, d is the waveguide half width, n_1 denotes the waveguide core refractive index and n_2 is the cladding index, $g(n_1,n_2)$ and $f_e(n_1,n_2,L_c)$ are dimensionless factors that are associated with waveguide geometry and material properties. The detailed expressions for these factors can be found in [35]. By plugging in the values of our GeSbSe waveguide, we plotted the scattering loss relation with various roughness values under several different roughness correlation lengths

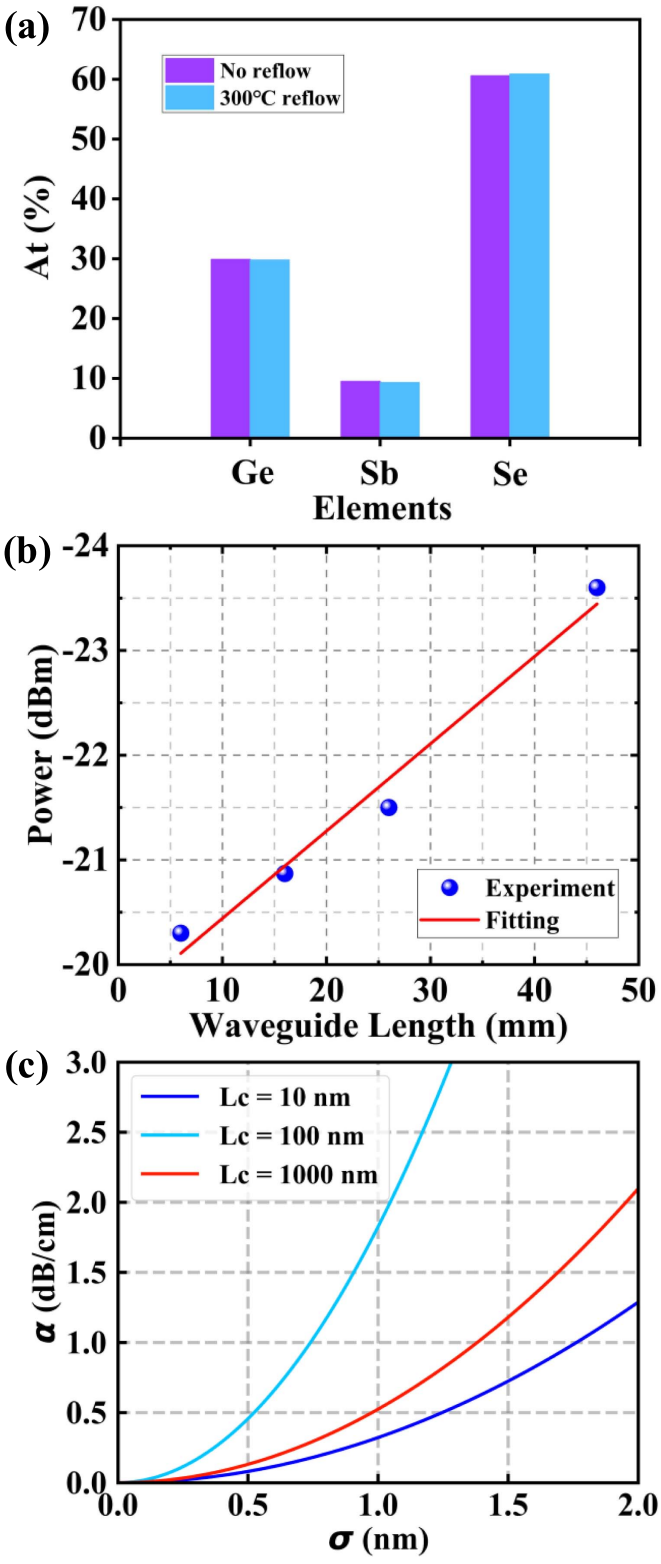

Figure 5. (a) normalized EDS elemental analysis of the waveguide; (b) waveguide loss extraction plot; and (c) numerical simulation result of waveguide loss with roughness mean square deviation.

in figure 5(c). Our analysis revealed that beyond the absolute magnitude of surface roughness, its correlation length exerts a significant influence on overall scattering loss. This implies that minimizing scattering loss requires a multifaceted approach considering both the roughness value and its spatial distribution.

Apart from the scattering loss addressed in this work, other loss factors include waveguide sidewall passivation polymer absorption, impurity atom-induced mid-gap state aborption, and scattering from material index variation along the wafer. To achieve even lower loss, developing effective approaches to remove all possible parasitic coatings as well as high-quality material manufacturing and deposition technology are demanded. With a zero-defect, parasitic coating-free, phase-pure, and index-invariant waveguide, we believe GeSbSe has the potential to achieve an ultra-low loss comparable to that in SiN_x and promote exciting application demonstrations in the mid-IR [36].

5. Conclusion

In conclusion, we experimentally demonstrated that the adoption of an oxide sacrificial layer and waveguide thermal reflow is a successful approach to eliminating etching residues and creating smooth waveguide sidewalls. The technology allows the reduction of waveguide loss down to 0.8 dB cm^{-1}, representing the best result in GeSbSe small core and high index contrast waveguides. Elemental analysis indicated that this technology does not degrade the waveguide. This fabrication process is not compositional sensitive and is equally applicable to other chalcogenide glass. We foresee this technology promoting low-loss waveguides being deployed as mid-IR light sources as well as sensing platforms, supporting fully lab-on-a-chip sensor systems.

Data availability statement

All data that support the findings of this study are included within the article (and any supplementary files).

Acknowledgments

This work was funded by National Key R&D Program of China under Grant No. 2021ZD0109904, and National Natural Science Foundation of China under Grant No. 62305304. The authors acknowledge the Nano Fabrication Center of Zhejiang Laboratory and the Center for Micro/Nano Fabrication in Westlake University for chalcogenide glass waveguides fabrication and characterization.

ORCID iD

Qingyang Du https://orcid.org/0000-0002-1424-356X

References

[1] Tran M A, Huang D, Komljenovic T, Peters J, Malik A and Bowers J E 2018 Ultra-low-loss silicon waveguides for heterogeneously integrated silicon/III–V photonics *Appl. Sci.* **8** 1139

[2] Ye Z, Jia H, Huang Z, Shen C, Long J, Shi B, Luo Y-H, Gao L, Sun W and Guo H 2023 Foundry manufacturing of tight-confinement, dispersion-engineered, ultralow-loss silicon nitride photonic integrated circuits *Photon. Res.* **11** 558–68

[3] Powell K, Shams-Ansari A, Desai S, Austin M, Deng J, Sinclair N, Lončar M and Yi X 2020 High-Q suspended optical resonators in 3C silicon carbide obtained by thermal annealing *Opt. Express* **28** 4938–49

[4] Gallacher K, Millar R, Griškevičiūte U, Baldassarre L, Sorel M, Ortolani M and Paul D 2018 Low loss Ge-on-Si waveguides operating in the 8–14 μm atmospheric transmission window *Opt. Express* **26** 25667–75

[5] Chang L, Boes A, Pintus P, Xie W, Peters J D, Kennedy M, Jin W, Guo X-W, Yu S-P and Papp S B 2019 Low loss (Al) GaAs on an insulator waveguide platform *Opt. Lett.* **44** 4075–8

[6] Ye Z, Zhao P, Karlsson M and Andrekson P A 2022 Ultralow-loss silicon nitride waveguides for parametric amplification *Optical Fiber Communication Conf.* (Optica Publishing Group) pp W4J–3

[7] Shen B, Chang L, Liu J, Wang H, Yang Q-F, Xiang C, Wang R N, He J, Liu T and Xie W 2020 Integrated turnkey soliton microcombs *Nature* **582** 365–9

[8] Rebolledo-Salgado I, Ye Z, Christensen S, Lei F, Twayana K, Schröder J and Zelan M 2022 Coherent supercontinuum generation in all-normal dispersion Si_3N_4 waveguides *Opt. Express* **30** 8641–51

[9] Liu Y, Qiu Z, Ji X, Lukashchuk A, He J, Riemensberger J, Hafermann M, Wang R N, Liu J and Ronning C 2022 A photonic integrated circuit–based erbium-doped amplifier *Science* **376** 1309–13

[10] Lin H, Luo Z, Gu T, Kimerling L C, Wada K, Agarwal A and Hu J 2017 Mid-infrared integrated photonics on silicon: a perspective *Nanophotonics* **7** 393–420

[11] Heck M J, Bauters J F, Davenport M L, Spencer D T and Bowers J E 2014 Ultra-low loss waveguide platform and its integration with silicon photonics *Laser Photon. Rev.* **8** 667–86

[12] Coddington I, Newbury N and Swann W 2016 Dual-comb spectroscopy *Optica* **3** 414–26

[13] Kita D M, Michon J and Hu J 2020 A packaged, fiber-coupled waveguide-enhanced Raman spectroscopic sensor *Opt. Express* **28** 14963–72

[14] Eggleton B J, Luther-Davies B and Richardson K 2011 Chalcogenide photonics *Nat. Photon.* **5** 141–8

[15] Ródenas A, Martin G, Arezki B, Psaila N, Jose G, Jha A, Labadie L, Kern P, Kar A and Thomson R 2012 Three-dimensional mid-infrared photonic circuits in chalcogenide glass *Opt. Lett.* **37** 392–4

[16] Gholipour B, Elliott S R, Müller M J, Wuttig M, Hewak D W, Hayden B E, Li Y, Jo S S, Jaramillo R and Simpson R E 2023 Roadmap on chalcogenide photonics *J. Phys. Photonics* **5** 012501

[17] Dai S, Wang Y, Peng X, Zhang P, Wang X and Xu Y 2018 A review of mid-infrared supercontinuum generation in chalcogenide glass fibers *Appl. Sci.* **8** 707

[18] Zhang B, Xia D, Zhao X, Wan L and Li Z 2023 Hybrid-integrated chalcogenide photonics *Light Adv. Manuf.* **4** 1–16

[19] Du Q, Huang Y, Li J, Kita D, Michon J, Lin H, Li L, Novak S, Richardson K and Zhang W 2016 Low-loss photonic device in Ge-Sb-S chalcogenide glass *Opt. Lett.* **41** 3090–3

[20] Hô N, Phillips M C, Qiao H, Allen P J, Krishnaswami K, Riley B J, Myers T L and Anheier N C 2006 Single-mode low-loss chalcogenide glass waveguides for the mid-infrared *Opt. Lett.* **31** 1860–2

[21] McMillen B, Zhang B, Chen K P, Benayas A and Jaque D 2012 Ultrafast laser fabrication of low-loss waveguides in chalcogenide glass with 0.65 dB/cm loss *Opt. Lett.* **37** 1418–20

[22] Madden S, Choi D-Y, Bulla D, Rode A V, Luther-Davies B, Ta'eed V G, Pelusi M and Eggleton B J 2007 Long, low loss etched As_2S_3 chalcogenide waveguides for all-optical signal regeneration *Opt. Express* **15** 14414–21

[23] Hu J, Feng -N-N, Carlie N, Petit L, Agarwal A, Richardson K and Kimerling L 2010 Optical loss reduction in high-index-contrast chalcogenide glass waveguides via thermal reflow *Opt. Express* **18** 1469–78

[24] Lee D H, Choo S J, Jung U, Lee K W, Kim K W and Park J H 2014 Low-loss silicon waveguides with sidewall roughness reduction using a SiO_2 hard mask and fluorine-based dry etching *J. Micromech. Microeng.* **25** 015003

[25] Zhang H, Zhang J, Chen S, Song J, Kee J S, Yu M and Lo G-Q 2011 CMOS-compatible fabrication of silicon-based sub-100 nm slot waveguide with efficient channel-slot coupler *IEEE Photonics Technol. Lett.* **24** 10–12

[26] Kim Y-J, Hong S-H, Lee J-S, Jeon S-J, Choi W J and Choi Y-W 2022 Thermal reflow effect in multi-mode waveguide of S-bend resonator with mode discrimination *IEEE Photon. J.* **14** 1–6

[27] Prabhakar K and Reano R M 2022 Fabrication of low loss lithium niobate rib waveguides through photoresist reflow *IEEE Photon. J.* **14** 1–8

[28] Zhao Y, Li C, Guo P, Zhang W, Xu P and Zhang P 2019 Exploration of lift-off Ge-As-Se chalcogenide waveguides with thermal reflow process *Opt. Mater.* **92** 206–11

[29] Grayson M, Xu B, Shanavas T, Zohrabi M, Bae K, Gopinath J T and Park W 2022 Fabrication and characterization of high quality GeSbSe reflowed and etched ring resonators *Opt. Express* **30** 31107–21

[30] Zhou J, Du Q, Xu P, Zhao Y, Lin R, Wu Y, Zhang P, Zhang W and Shen X 2018 Large nonlinearity and low loss Ge-Sb-Se glass photonic devices in near-infrared *IEEE J. Sel. Top. Quantum Electron.* **24** 1–6

[31] Vanier F, Rochette M, Godbout N and Peter Y-A 2013 Raman lasing in As_2S_3 high-Q whispering gallery mode resonators *Opt. Lett.* **38** 4966–9

[32] Ma P, Choi D-Y, Yu Y, Gai X, Yang Z, Debbarma S, Madden S and Luther-Davies B 2013 Low-loss chalcogenide waveguides for chemical sensing in the mid-infrared *Opt. Express* **21** 29927–37

[33] Oehrlein G S, Phaneuf R J and Graves D B 2011 Plasma-polymer interactions: a review of progress in understanding polymer resist mask durability during plasma etching for nanoscale fabrication *J. Vac. Sci. Technol.* B **29** 010801

[34] Zhu Y, Wan L, Chen Z, Yang Z, Xia D, Zeng P, Song J, Pan J, Feng Y and Zhang M 2020 Effects of shallow suspension in low-loss waveguide-integrated chalcogenide microdisk resonators *J. Lightwave Technol.* **38** 4817–23

[35] Payne F P and Lacey J P 1994 A theoretical analysis of scattering loss from planar optical waveguides *Opt. Quantum Electron.* **26** 977–86

[36] Carlie N, Musgraves J D, Zdyrko B, Luzinov I, Hu J, Singh V, Agarwal A, Kimerling L C, Canciamilla A and Morichetti F 2010 Integrated chalcogenide waveguide resonators for mid-IR sensing: leveraging material properties to meet fabrication challenges *Opt. Express* **18** 26728–43